Pergamon

0301-9322(95)00032-1

Int. J. Multiphase Flow Vol. 21, No. 6, pp. 1025–1036, 1995

0301-9322/95 $9.50 + 0.00

DIRECT CONTACT HEAT TRANSFER BETWEEN TWO IMMISCIBLE LIQUIDS FLOWING IN A HORIZONTAL CONCENTRIC ANNULUS

M. K. SHAHIDI and T. A. ÖZBELGE

Department of Chemical Engineering, Middle East Technical University, Ankara 06531, Turkey

(Received 26 April 1994; in revised form 16 April 1995)

Abstract—Direct contact heat transfer between water and a heat transfer oil was investigated under non-boiling conditions in co-current turbulent flow through a horizontal concentric annulus. The ratio of the inner pipe diameter to the outer pipe diameter (aspect ratio) $\kappa = 0.730$–0.816; total liquid velocity (mixture velocity) $V_T = 0.42$–1.1 m/s; inlet oil temperature $T_{oi} = 38$–94°C; oil volume fraction in the flowing mixture $\phi_o = 0.25$–0.75 were varied and their effects on the overall volumetric heat transfer coefficient U_v were determined at constant interfacial tension of 48 dynes/cm.

It was found that, in each concentric pipe set, the overall volumetric heat transfer coefficient increased with increasing dispersed phase volume fraction at each constant mixture velocity and reached a maximum at around $\phi_o = \phi_w \approx 0.5$. The maximum U_v values increased with increasing total liquid velocity and decreasing aspect ratio of the annulus. The volumetric heat transfer coefficient was also found to increase with increasing inlet oil temperature and increasing total liquid velocity but to decrease with length along the test section keeping all other parameters constant. Empirical expressions for the volumetric heat transfer coefficient were obtained within the ranges of the experimental parameters.

Key Words: concentric annulus, immiscible liquids, turbulent flow, direct contact heat transfer

1. INTRODUCTION

A growing interest in two-phase flows is evidenced by a recent increase in publications dealing with the gas–liquid, liquid–liquid and liquid–solid flows. Two-phase flows are of importance in petroleum production, pipeline transportation, transport reactors of chemical or nuclear type and evaporator–condenser designs. While much attention has been given to gas–liquid flows, little has been devoted to liquid–solid and liquid–liquid flows, especially in different geometries. Depending on the geometry of the system and the operating conditions, the shear stresses exerted by the continuous phase on the surface of drops will affect the flow characteristics at the interphase which, in turn, will change the heat transfer rate.

Most studies on two-phase flows to date are concerned with circular pipes and little is known about their flow and heat transfer characteristics in non-circular channels. However, in practice, many heat exchanger applications need consideration of an annular configuration; in other applications, the knowledge for the two-phase flow in rectangular and triangular geometries may be required. Therefore it is desired to obtain experimental data in different geometries not only for a better understanding of the inherent flow behavior and heat transfer mechanism but also to make use of the information compiled from the investigation of circular pipes so far made, by using the hydraulic diameter concept. Considering the direct-contact heat transfer of immiscible liquids, numerous extensive reviews of experimental and theoretical investigations were published over the past years, most notably by Sideman (1966), Kehat & Sideman (1971) and Wilke *et al.* (1963).

Some of the relatively recent work can be mentioned here. Moresco & Marshall (1980) carried out experiments in a spray column with oil as the dispersed phase and pure water as the continuous phase. They measured the local temperatures of continuous and dispersed phases and found that, during drop formation and release, the internal heat transfer coefficients were very much higher than those predicted by Handlose & Baron (1957). In fact, during this process the major resistance to heat transfer was found to be in the continuous phase and not, as usually assumed, in the dispersed phase (Sideman & Shabatai 1964). Grover & Knudsen (1955) determined the rate of heat transfer between a petroleum solvent and water in a circular pipe used as a co-current heat

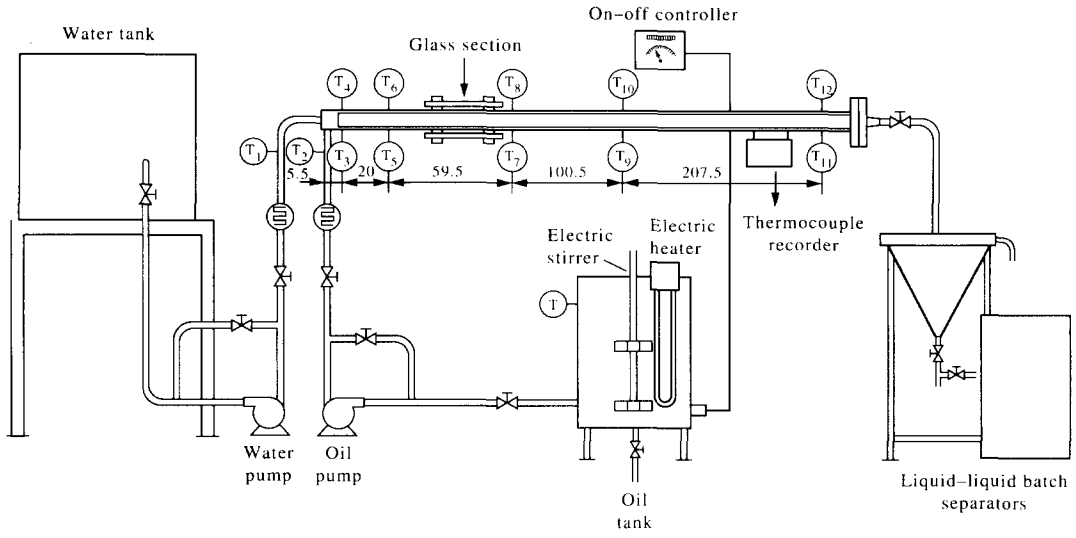

Figure 1. Schematic of the experimental set-up.

exchanger. Better dispersion gave higher volumetric heat transfer coefficients. Porter *et al.* (1968) and Yalvaç (1974) investigated the direct contact heat transfer between oil and water in turbulent horizontal pipe flow using a semi-empirical method of correlating the data. Köksal (1980) performed a similar study with oil and salty water in turbulent pipe flow. Takahashi *et al.* (1981) studied the thermo-hydrodynamic characteristics of a co-current stratified flow of liquid metal and water in a horizontal rectangular channel. Leib *et al.* (1978) investigated heat transfer to annular laminar flow of two immiscible liquids (kerosene–water system) in a vertical pipe. The outer phase was kerosene around the inner liquid phase, which was water, and it acted as a thermal insulating layer between the electrically heated wall and water flowing in the core region of the pipe.

As can be seen from this review, studies relating to the direct contact heat exchange of immiscible liquids flowing in an annulus have not been found in the literature, and so the objective of the present study was to investigate this problem in concentric annuli.

2. EXPERIMENTAL WORK

The immiscible liquids used in this study are water and a heating oil manufactured by British Petroleum with a trade name of BP-Transcal-N.

2.1. Experimental set-up

A schematic diagram of the apparatus is given in figure 1. It consisted of a large water tank, a horizontal annulus, a liquid–liquid separator tank, oil and water pumps and an oil tank equipped with a 3 kW electrical heater, an electrical stirrer and a resistance thermometer connected to a temperature controller to keep the inlet oil temperature constant at the desired value. The test section was a horizontal concentric annulus made of galvanized iron approximately 4 m in length. A short pipe section of 25 cm in length, close to the entrance region, was made of glass having the same diameter as that of the outer pipe to be used for visual and photographic observations of flow patterns, formation and size of drops of the dispersed phase. The oil and water streams

Table 1. Characteristics of concentric pipe sets

Pipe set	Material of construction	D_{oi} (mm)	D_{io} (mm)	κ	A_f (m^2)	D_h (mm)
I	Inner pipe: galvanized iron Outer pipe: galvanized iron	51.5	42	0.816	6.9762×10^{-4}	9.5
II	Inner pipe: galvanized iron Outer pipe: galvanized iron	35.6	26	0.730	4.6445×10^{-4}	9.6
III	Inner pipe: copper Outer pipe: galvanized iron	35.6	28	0.787	3.7963×10^{-4}	7.6

were introduced into a very short pipe section of 2 cm in length where they hit each other at an angle so that a good dispersion and a proper mixing of two liquids before entering the annulus was provided. The flow rates were measured by previously calibrated orifice meters. The initial temperatures of both phases were measured before the mixing section of the annulus. Flow rates of liquids were controlled by the valves on the by-pass lines of the pumps. The temperature data were taken by fast response thermocouples and multi-channel recorder with a scale between 0–100°C. Iron–Constantan thermocouples of 0.5 mm in diameter were mounted at five different locations corresponding to the entry lengths of 5.5, 25.5, 85.0, 185.5, and 393.0 cm along the annulus. At each location, two thermocouples were placed at the upper and the lower parts of the annulus with respect to its horizontal central axis. The details for the concentric pipe sets are given in table 1, where D_{oi} is the inside diameter of the outer pipe, D_{io} is the outside diameter of the inner pipe, κ is the aspect ratio, A_f is the annular flow area and D_h is the hydraulic diameter of the annulus.

The concentricity of each pipe set was ensured by placing triangular blocks welded on the outer surface of the inner pipe at the apex of each block. Three blocks were situated 120° apart from each other at each of the three cross-sections along the annulus so that the inner horizontal pipe would not bend in the middle due to the gravitational force.

2.2. *Experimental procedure*

Orifice meters were calibrated separately for each fluid during its flow solely through the annulus. These calibrations were repeated for the flow of oil and water mixtures at different proportions through the annulus and were related to the volume fractions of the phases in the flowing mixture by collecting a sample of liquid mixture from the exit of the annulus within a certain time interval and allowing the liquids to separate in a graduated flask.

At the start of each experimental run, the temperature of the oil in the tank was set and it was allowed to reach the desired oil temperature. The mass flow rates of oil and water required to yield the desired volume fraction of oil ϕ_o and total liquid velocity V_T were calculated from the pairs of equations given in the appendix, which were derived for each concentric pipe set. These calculated flow rates of oil and water were adjusted manually using the calibration curves of the corresponding orifice meters. Both liquids were separately pumped into the test section at the same time and mixed in a short pipe section before entering the annulus in which they were caused to flow co-currently and turbulently by exchanging heat. The inlet oil and water temperatures were measured before mixing and the thermocouple readings at five different entry lengths were recorded within 15 s after turning the mixer and the pumps off and closing the end of the test section by a valve to avoid leakage of any liquid from the system. At that time, the liquids formed two separate layers of oil and water in the annulus and as the upper group of thermocouples measured the oil temperatures, the bottom group of thermocouples measured the water temperatures at the specified lengths along the annulus. During turbulent two-phase flow, the liquids were dispersed in each other and this caused difficulties in obtaining reliable temperature measurements. Therefore the above-given procedure was followed. The additional temperature readings were also taken within 30 s after the first set of temperature readings in each run to estimate the effect of continued heat transfer during the separation of the phases after the flow was stopped. When an experimental run was completed, the oil and water annular flow was followed by the separation of two liquids in a separator funnel. The heating oil was returned to the oil tank while the water was discarded after separation. During each experiment, the oil volume fraction was checked by collecting a sample of flowing liquid mixture from the exit of the annulus into a graduated flask where the volumes of oil and water phases were measured after separation. The experimental data in this study were obtained on a batch basis due to problems associated with inadequate liquid–liquid separation.

In the heat transfer experiments, the inlet oil temperature was varied between 38 and 94°C, whereas the inlet water temperature varied between 15 and 22°C. The range of total liquid velocity was from 0.4 to 1.1 m/s. The oil volume fraction was varied between 0.25 and 0.75. The surface tensions of oil and water were measured at room temperature (~20°C) as 43 and 75 dynes/cm, respectively, and the interfacial tension as 48 dynes/cm. The pertinent physical properties of BP-Transcal-N are listed in table 2.

Table 2. Physical properties of BP-Transcal-N oil

Temperature (°C)	Density (g/cm³)	Thermal conductivity (kcal/m h °C)	Viscosity (centistokes)
25	0.865	0.1140	50.0
50	0.814	0.1250	18.0
75	0.830	0.1200	8.0
100	0.815	0.0095	4.5

2.3. Calculation of volumetric heat transfer coefficient

Heat transferred between the two phases can be written as follows:

$$Q_o = Q'_w = Q_w + Q_{loss}, \quad [1]$$

where $Q_w = \dot{m}_w Cp_w \Delta T_w$, $Q_o = \dot{m}_o Cp_o \Delta T_o$, and Cp_w and Cp_o are heat capacities of water and oil respectively. Since the heat loss was less than 1% of total heat transfer, its effect was considered within the experimental error. The average of the heat taken up by the water Q_w and that given up by the oil Q_o, divided by the volume of the test section V, and the logarithmic mean temperature difference were used to calculate the volumetric heat transfer coefficient U_v:

$$UA/V = \frac{(Q_w + Q_o)/2V}{(\Delta T_{in} - \Delta T_{out})/\ln(\Delta T_{in}/\Delta T_{out})}, \quad [2]$$

where $U_v = UA/V$, $\Delta T_{in} = T_{oi} - T_{wi}$ (difference between inlet oil and water temperatures) and $\Delta T_{out} = T_{oo} - T_{wo}$ (difference between outlet oil and water temperatures).

3. RESULTS AND DISCUSSIONS

Experimental data were obtained in a variety of flow conditions to study the effects of oil volume fraction, total liquid velocity, inlet oil temperature and aspect ratio.

In the experiments, the temperature of each phase could not be measured right at the moment when the flow was stopped while the droplets were in the dispersed form. The first temperature measurements were taken within 15 s after the flow stopped. This time duration was longer than the time necessary for the separation of the phases. The amount of heat transfer during the phase separation was estimated to be almost equal to that during the time between the first temperature measurements and the temperature measurements recorded within 30 s after the first temperature readings, assuming the same heat flux between the phases during and after the separation. When the amount of heat transfer during the phase separation was compared with that during the entire experiment, it was found that the ratio of the heat transferred during the phase separation to the total heat transferred varied between 0.01 and 0.03 for the range of the observed droplet sizes and the estimated separation times of the phases in the present experimental work. Each experiment

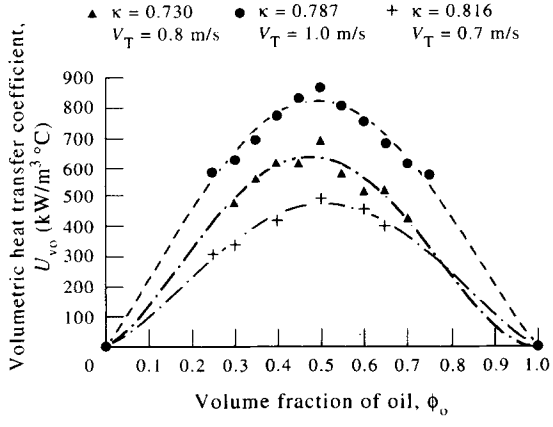

Figure 2. Plot of U_{vo} vs ϕ_o.

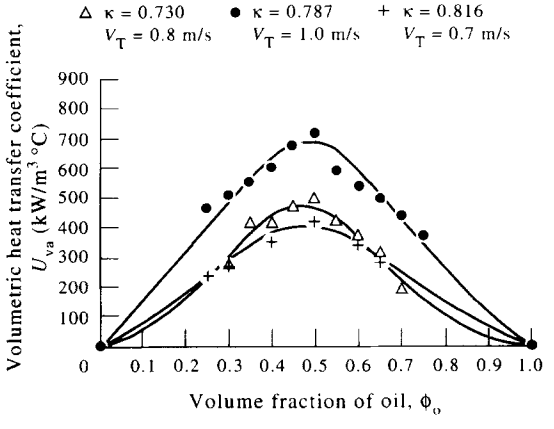

Figure 3. Plot of U_{va} vs ϕ_o.

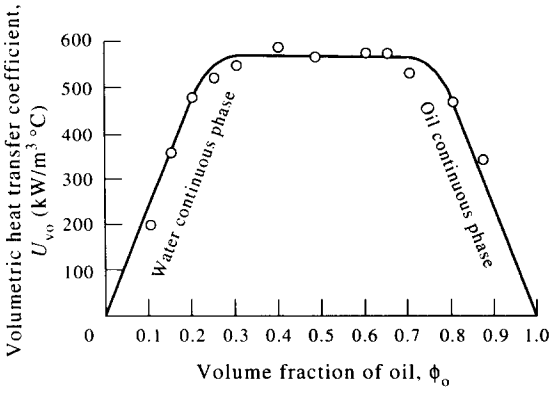

Figure 4. Plot of U_{vo} vs ϕ_o in a pipe for $A_f = 1.29\,cm^2$, $V_T = 2.09$ m/s and $T_{oi} = 73$°C (Yalvaç 1974).

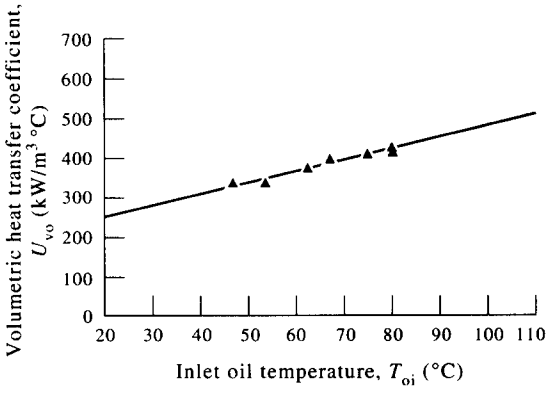

Figure 5. Plot of U_{vo} vs T_{oi} for $\kappa = 0.816$, $V_T = 0.7$ m/s, $\phi_o = 0.4$.

was repeated two or three times to check the reproducibility of the results. The maximum variation in the volumetric heat transfer coefficients between the repeated runs was 10%.

3.1. Effect of oil volume fraction

The calculated results of the volumetric heat transfer coefficients at different oil volume fractions from 0.0 to 1.0, keeping the total liquid velocity, the inlet oil temperature and the aspect ratio constant, are given in figures 2 and 3. Figure 2 shows the effect of oil volume fraction on the volumetric heat transfer coefficients U_{vo}, calculated over the total length of the annulus ($L = 3.93$ m) including the mixing section (i.e. a pipe section of 2 cm long) just before the annulus. Figure 3 represents the same relationship for volumetric heat transfer coefficients U_{va}, calculated over the length of annulus ($L = 3.875$ m) excluding the mixing section for the same runs. The difference between figures 2 and 3 for the same κ and V_T originated from the different inlet oil temperatures to the mixing section ($T_{oi} \sim 70$–75°C and $T_{wi} \sim 15$–22°C) and to the annulus after the mixing section ($T_{oi} \sim 40$–60°C and $T_{wi} \sim 20$–40°C) in each run, and it was not because of the changing heat transfer mechanism in the system. Further details are given elsewhere (Khatib Shahidi 1994).

The powers of the pumps limited the investigator to operate at different values of the total liquid velocity (mixture velocity) in each concentric pipe set which would allow to cover the widest possible range of oil volume fraction at a constant V_T. It was found that in each concentric pipe set, at any chosen value of the total liquid velocity, the volumetric heat transfer coefficient increased with increasing dispersed phase volume fraction and reached a maximum at around $\phi_o = \phi_w \approx 0.5$ (figures 2 and 3). If this result is compared with those of previous studies (Porter *et al.* 1968; Yalvaç 1974; Köksal 1980) in pipe flow, it is observed in figure 4 (Yalvaç 1974) that the volumetric heat transfer coefficient increases with the dispersed phase concentration up to $\phi_o = \phi_w \cong 0.25$ and then it remains constant between 0.25 and 0.75 oil volume fraction. In this region of constant heat

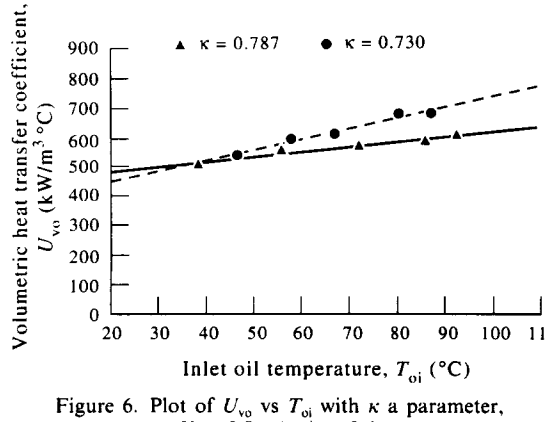

Figure 6. Plot of U_{vo} vs T_{oi} with κ a parameter, $V_T = 0.8$ m/s, $\phi_o = 0.4$.

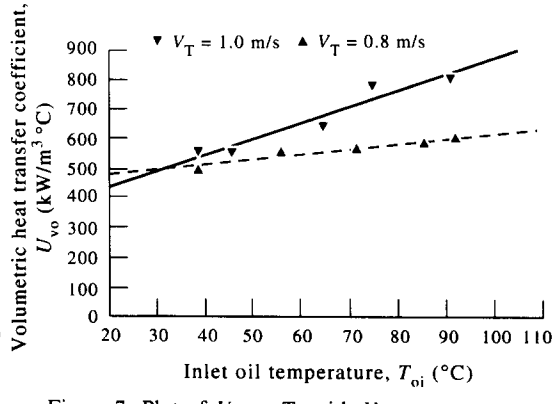

Figure 7. Plot of U_{vo} vs T_{oi} with V_T a parameter, for $\kappa = 0.787$, $\phi_o = 0.4$.

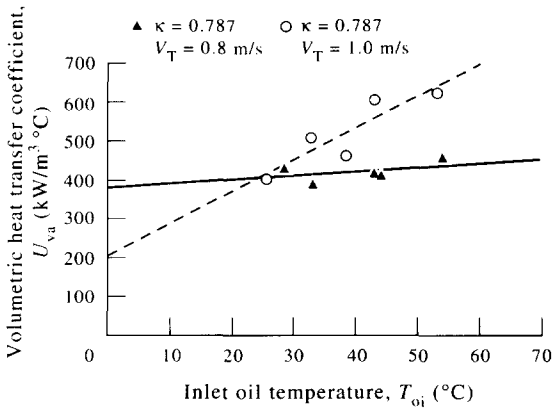

Figure 8. Plot of U_{va} vs T_{oi} with V_T a parameter, $\phi_o = 0.4$.

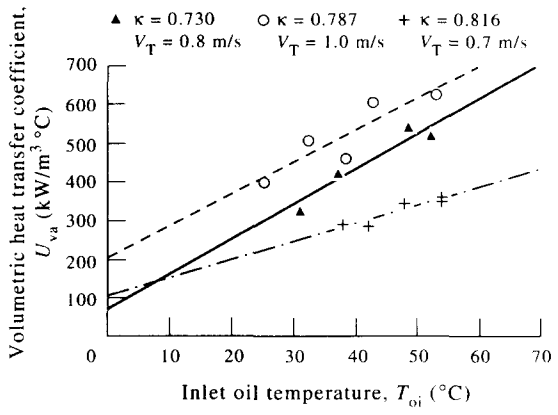

Figure 9. Plot of U_{va} vs T_{oi} with V_T and κ parameters, $\phi_o = 0.4$.

transfer coefficient, the rate of increase in the interfacial area due to the increasing concentration of the dispersed phase was claimed to be counterbalanced by the increasing rate of coalescence. Porter *et al.* (1968) reported that the transition point from a water continuous phase to an oil continuous phase was approximately determined at $\phi_w \approx 0.3$ in pipe flow, though this transition was not clear-cut. However, in the present work, this point was clearly observed at around $\phi_o = \phi_w \approx 0.5$, where a maximum value of U_{vo} was expected, since U_{vo} increased with the dispersed phase concentration. This can be qualitatively explained by the unequal shear stresses exerted on the drops located in the annulus by the inner and the outer pipe surfaces (Bird *et al.* 1960) which cause the deformation of spherical liquid drops to pear-shaped drops and the break-up of drops into droplets. Thus, the rate of coalescence decreases and the interfacial area of the dispersed phase per unit volume of the test section continues to increase with the increasing dispersed phase volume fraction. Therefore, U_{vo} values do not remain constant and increase to their maximum values occurring at $\phi_o = \phi_w \approx 0.5$. This effect becomes more significant the higher the κ value decreases where the difference between the unequal shear stresses increases yielding the higher heat transfer coefficients.

3.2. *Effect of inlet oil temperature*

Heat transfer coefficients were calculated at various inlet oil temperatures (38–94°C), all other parameters being held constant. The results are given in figures 5–9 which show that the volumetric heat transfer coefficient increases almost linearly with the inlet oil temperature. Increasing inlet oil temperature causes a decrease in oil density and oil viscosity which are the two important variables affecting the Reynolds number. However, the relative decrease in viscosity with respect to density

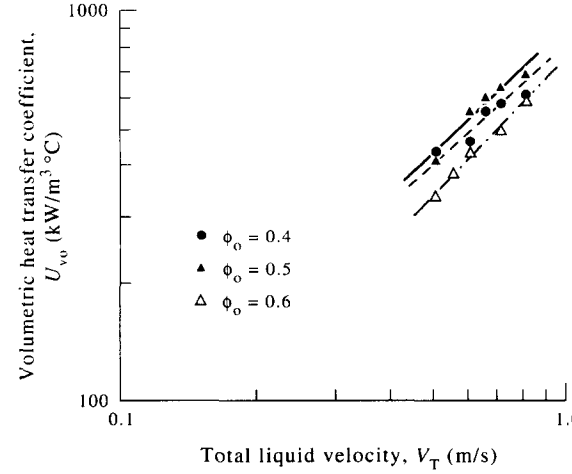

Figure 10. Plot of U_{vo} vs V_T with ϕ_o a parameter, for $\kappa = 0.730$.

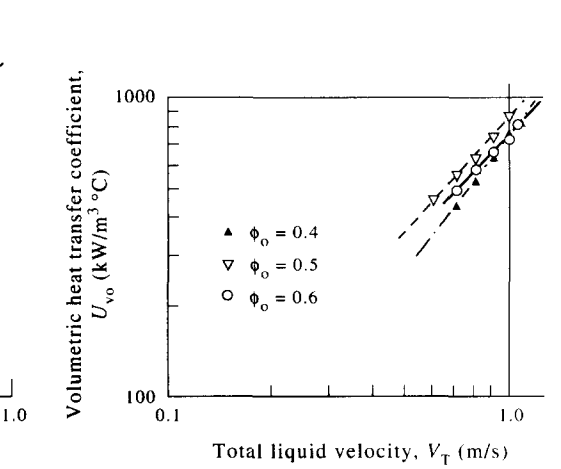

Figure 11. Plot of U_{vo} vs V_T with ϕ_o a parameter, for $\kappa = 0.787$.

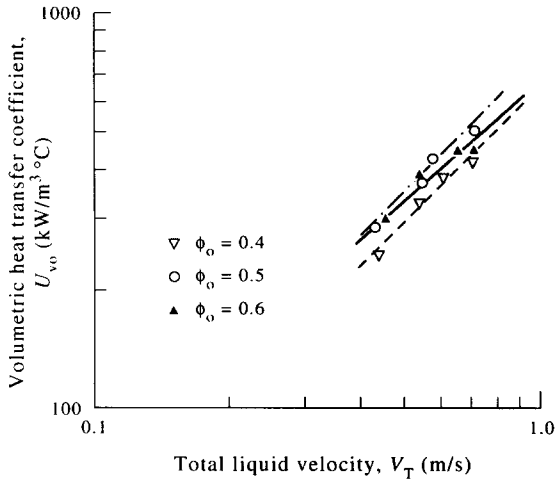

Figure 12. Plot of U_{vo} vs V_T with ϕ_o a parameter, for $\kappa = 0.816$.

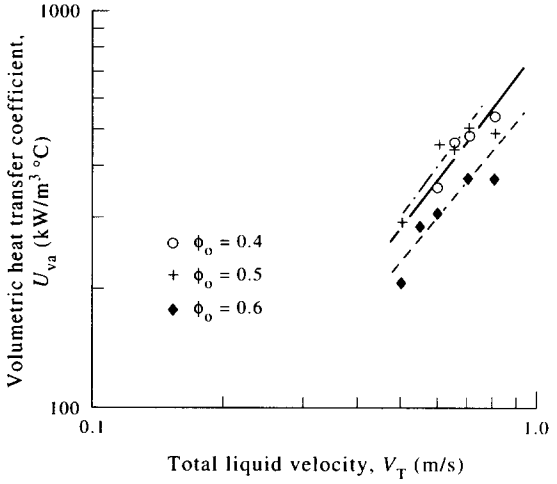

Figure 13. Plot of U_{va} vs V_T with ϕ_o a parameter, for $\kappa = 0.730$.

is larger and so at higher temperatures the two-phase flow becomes more turbulent giving larger volumetric heat transfer coefficients. At the same time as inlet oil temperature increases for a constant water inlet temperature, the driving force for heat transfer increases.

3.3. Effect of total liquid velocity and aspect ratio

The plots of volumetric heat transfer coefficient vs total liquid velocity, keeping all other parameters constant, are shown in figures 10–15. As it is observed from these figures, U_{vo} and U_{va} increase almost linearly with total liquid velocity for each κ and ϕ_o value. This can be explained with the increasing degree of turbulence as a result of higher shear rates developed in annular flow compared with those developed in pipe flow, so that in turn a better mixing is achieved between two immiscible liquids. Therefore, in annular flow the rate of coalescence will be lower than that in the pipe flow. This will result in smaller droplet sizes and greater deformation of the droplets in the dispersed phase. Consequently, interfacial area for direct contact heat transfer between two liquids becomes larger.

For the purpose of comparison, figures 10–12 were plotted at the aspect ratios of 0.730, 0.787 and 0.816, respectively, with the oil volume fraction being a parameter, and straight lines with slopes ranging from 0.9 to 1.5 were obtained. The slopes of the lines obtained for the annulus with the smallest cross-sectional area and κ value of 0.787 (figure 11) are greater than those slopes observed in figures 10 and 12. This shows the increasing effect of liquid velocity on the volumetric

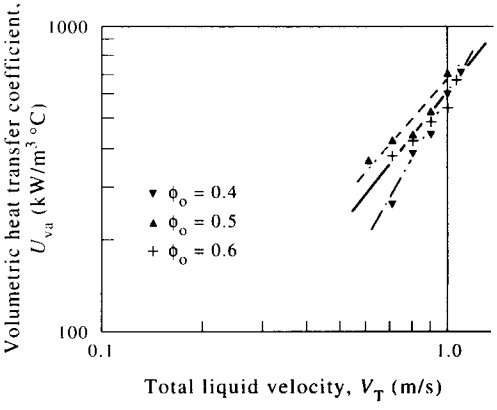

Figure 14. Plot of U_{va} vs V_T with ϕ_o a parameter, for $\kappa = 0.787$.

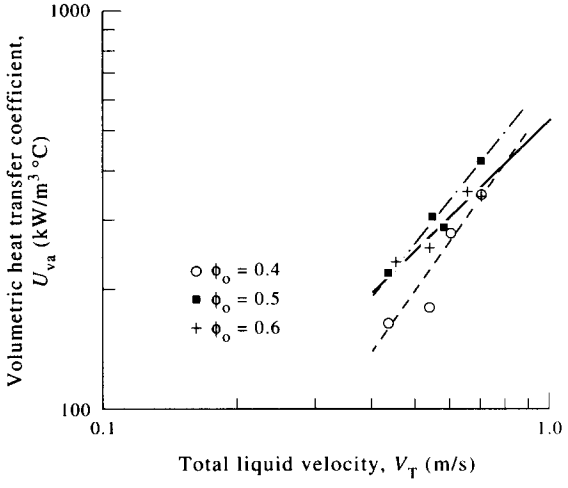

Figure 15. Plot of U_{va} vs V_T with ϕ_o a parameter, for $\kappa = 0.816$.

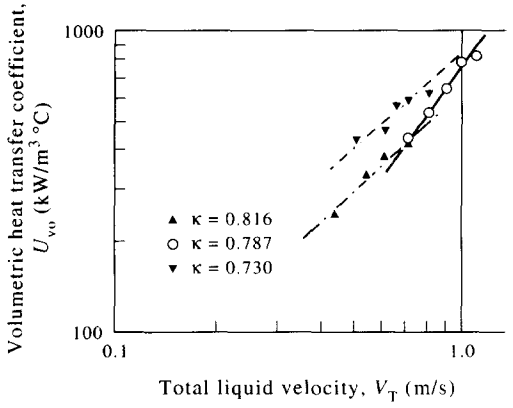

Figure 16. Plot of U_{vo} vs V_T with κ a parameter, for $\phi_o = 0.4$.

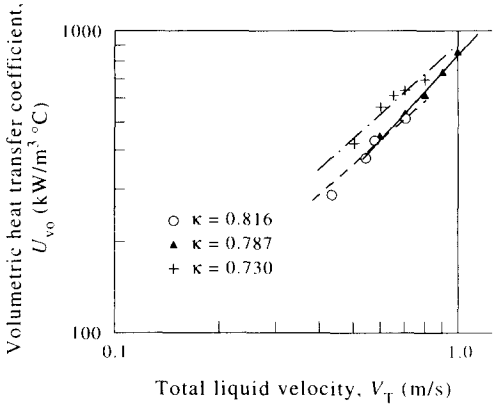

Figure 17. Plot of U_{vo} vs V_T with κ a parameter, for $\phi_o = 0.5$

heat transfer coefficient for this κ value of 0.787, but the magnitudes of U_{vo} values corresponding to $\kappa = 0.787$ are smaller than those obtained in the annulus with a κ value of 0.730. This indicates the dominant effect of the aspect ratio κ on the volumetric heat transfer coefficient over that of the liquid velocity within the range of experimental parameters. It is already known for the laminar flow through an annulus that the difference between the shear stresses applied by the fluid on the inner and outer walls increases with the decreasing κ value (Bird *et al.* 1960). The same behavior is also expected for turbulent regimes. This means that as the κ value decreases, the difference between the shear stresses exerted on the two wall-side peripheries of a drop in the annulus increases. This changes the shape and the rotational behavior of the drop and in turn enhances the heat transfer rate between the dispersed and the continuous phases.

In figures 10–12, the volumetric heat transfer coefficients for $\phi_o = 0.5$ are greater than those for 0.4 and 0.6 at each liquid velocity and the straight line for $\phi_o = 0.5$ represents the locus of maximum heat transfer coefficients obtained at each constant mixture velocity in each pipe set (e.g. maximum U_{vo} values at $\phi_o = 0.5$ and at different velocities in figure 2). The magnitude of maximum volumetric heat transfer coefficient increases with increasing velocity almost linearly on the log–log plots. The plots of U_{va} vs V_T (figures 13–15) show similar trends to those observed in figures 10–12.

In figures 16–18, the logarithmic plots of U_{vo} vs V_T are given for the oil volume fractions of 0.4–0.6, respectively, with the aspect ratio being a parameter. They all give straight lines. At each constant liquid velocity and each oil volume fraction, the highest volumetric heat transfer coefficients are obtained in pipe set II which has the smallest aspect ratio of 0.73. Apparently, the pipe set II created the most favorable flow patterns for the enhancement of direct contact heat transfer between immiscible liquids. When the behavior of dispersed and continuous phases were visually observed through the transparent section of the flow system, the following important points were noted.

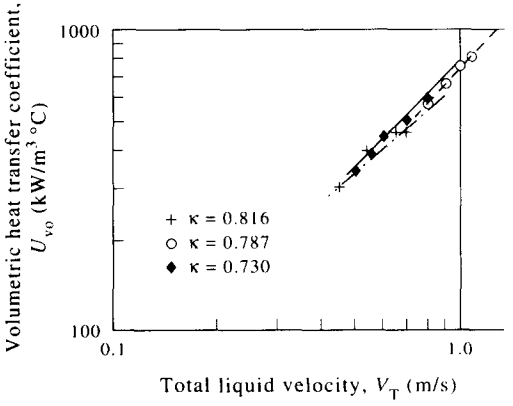

Figure 18. Plot of U_{vo} vs V_T with κ a parameter, for $\phi_o = 0.6$.

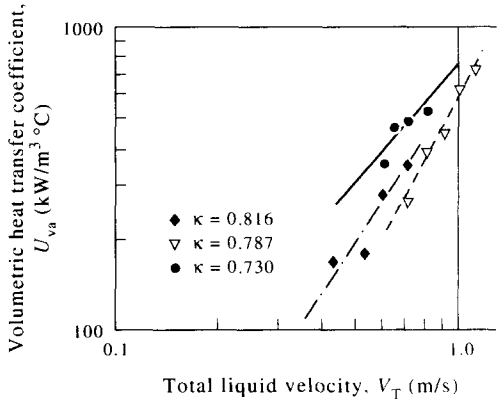

Figure 19. Plot of U_{va} vs V_T with κ a parameter, for $\phi_o = 0.4$.

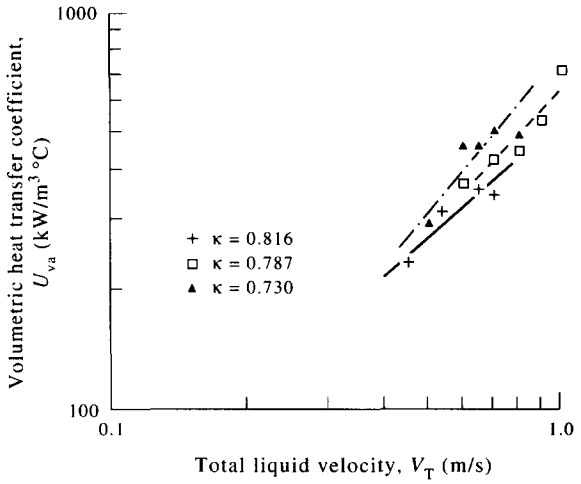

Figure 20. Plot of U_{va} vs V_T with κ a parameter, for $\phi_o = 0.5$.

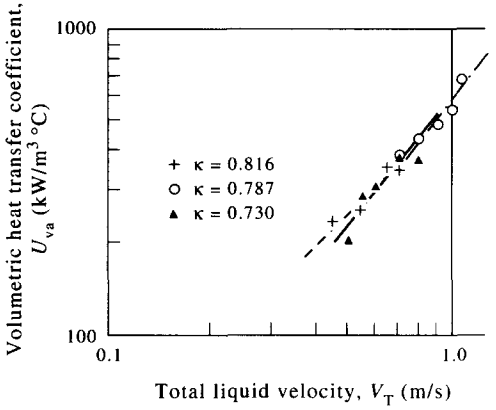

Figure 21. Plot of U_{va} vs V_T with κ a parameter, for $\phi_o = 0.6$.

At low flow velocities due to low shear, dispersion between the phases was low and the two phases flowed in a stratified manner. This behavior was observed in most of the runs performed for the largest κ value of 0.816 and the largest flow area.

When the flow area was decreased and the κ value was equal to 0.730, the velocity range was 0.5–0.8 m/s. In most of the runs a good dispersion was observed in each phase (when ϕ_o was less than 0.5, water was the continuous phase, and when ϕ_o was equal to or larger than 0.5, oil was the continuous phase). At lower velocity ranges partial stratification was observed and, while the upper phase consisted of dispersed water in oil, the lower phase consisted of dispersed oil in water. In dispersed–stratified flows, a significant deformation and elongation of the dispersed droplets in the flow direction was observed due to the shear stresses. The occurrence of the highest volumetric heat transfer coefficients in the pipe set with $\kappa = 0.730$ can be attributed to this type of flow pattern.

For the smallest flow area and medium κ value of 0.787, at high velocities fully dispersed flow was observed, but at low velocities stratified–dispersed flows were seen. During the runs performed in this pipe set, elongation of droplets was not significant and the shape of the droplets was spherical.

Figures 19–21 are the logarithmic plots of U_{va} vs V_T for oil volume fractions of 0.4–0.6 respectively, with the aspect ratio being a parameter. The same arguments about figures 16–18 can be repeated for figures 19–21.

3.4. Modeling studies

The following empirical model equations for direct contact volumetric heat transfer coefficients of immiscible liquids in turbulent flow through horizontal concentric annuli were obtained by applying regression methods (Marquardt 1963) on the same experimental data:

$$U_{vo} = 729.38\phi_o^{0.6} V_T^{1.19} \kappa^{-2.27}, \quad \text{for } 0 < \phi_o \leqslant 0.5, \qquad [3]$$

$$U_{vo} = 1132.2\,\phi_w^{0.67} V_T^{1.17} \kappa^{-0.78}, \quad \text{for } 0 < \phi_w \leqslant 0.5, \qquad [4]$$

where the constants 729.38 and 1132.2 have the units of kg/m$^{2.19}$ s$^{1.81}$ °C and kg/m$^{2.17}$ s$^{1.83}$ °C, respectively. The accuracies of these correlations [3] and [4] are ± 10% for the following intervals of the variables: total liquid velocity $V_T = 0.4$–1.1 m/s; aspect ratio $\kappa = 0.730$–0.816; inlet water temperature $T_{wi} = 15$–22°C; inlet oil temperature $T_{oi} = 50$–75°C.

In figure 2, the left and right branches of the curves with respect to the maximum U_{vo} values are represented by [3] and [4], respectively. In both branches, the powers of the dispersed phase volume fractions in [3] and [4] are very close which explains the symmetry of these curves. The closeness of the powers on the total liquid velocity terms in the two equations indicates almost the same effect of this parameter on U_{vo} in both branches. This can also be observed from log–log plots of U_{vo} vs V_T at the same κ value where the straight lines are almost parallel for different dispersed

phase volume fractions (figure 10 for $\kappa = 0.730$, figure 11 for $\kappa = 0.787$ and figure 12 for $\kappa = 0.816$).

Comparing the powers of κ in [3] and [4], it is obvious that the effect of κ is greater in the region where oil is the dispersed phase. The increasing shear stresses with the decreasing κ value can more easily deform oil droplets rather than water droplets. This can be explained with the functional relationship (Hinze 1955) between the Weber number $We = \rho_c V_T^2 D_h/\sigma$, the viscosity ratio of the immiscible liquid phases μ_c/μ_d, and the viscosity group defined by $\mu_d/\sqrt{\rho_d \sigma d_p}$, where μ, ρ and σ are the viscosity, density and the interfacial tension respectively. The subscripts c and d indicate the continuous and the dispersed phases, respectively. D_h is the pipe diameter or the hydraulic diameter depending on the geometry of the system and d_p is the diameter of the liquid globule or drop. It is described that the Weber number generally refers to the dynamic pressure set up in the continuous phase around the globule and that the critical Weber number is reached when the deformation or the break-up of the globule occurs. It is further stated that the critical Weber number occurs at lower values of the viscosity group as the viscosity of the continuous phase decreases. From this explanation it may be deduced that as the external force on the liquid drops increases with the decreasing κ value, oil drops in the water-continuous phase can be more easily deformed than the water drops in the oil-continuous phase. This is because, in the latter case, the occurrence of the critical Weber number for the deformation of the water drops corresponds to a higher value of the viscosity group due to the higher viscosity of the oil-continuous phase. In other words, the external force required to deform water drops in the oil phase should be greater to overcome the viscous forces.

Earlier heat transfer correlations obtained for pipe flow of immiscible liquids (Porter *et al.* 1968; Yalvaç 1974) were not valid within the ranges of the experimental parameters of this study, and so the present results obtained in the annuli could not be compared with the earlier work of the pipe flow by using the hydraulic diameter concept. Although the total liquid velocities used in the present experiments are lower than those used in the earlier studies of liquid–liquid direct contact heat transfer in the pipe flow, the volumetric heat transfer coefficients obtained in the annulus flow are higher than those of the pipe flow. The reason for this can be attributed to the deformation and break-up of the drops by the high shear stresses applied on the drops due to the characteristics of the annulus geometry which proved the advantage of using the annulus geometry in the multiphase exchangers.

4. CONCLUSIONS

In direct contact heat transfer of immiscible liquids in annuli, the experimental data show that volumetric heat transfer coefficient increases with increasing dispersed phase volume fraction and reaches a maximum at around $\phi_o = \phi_w \approx 0.5$ keeping all other parameters constant. The magnitude of this maximum coefficient at $\phi_o \approx 0.5$ and at a constant velocity increases with the increasing total liquid velocity of mixture and with decreasing aspect ratio. The volumetric heat transfer coefficients also increase with increasing inlet oil temperature while all the other parameters are held constant.

The following empirical equations for direct contact volumetric heat transfer coefficients of two immiscible liquids in turbulent flow through horizontal concentric annuli were obtained within maximum $\pm 10\%$ error margins for the given intervals of the experimental parameters:

$$U_{vo} = 729.38 \phi_o^{0.6} V_T^{1.19} \kappa^{-2.27}, \quad \text{for } 0 < \phi_o \leqslant 0.5,$$

$$U_{vo} = 1132.2 \phi_w^{0.67} V_T^{1.17} \kappa^{0.78}, \quad \text{for } 0 < \phi_w \leqslant 0.5,$$

for $V_T = 0.4$–1.1 m/s; $\kappa = 0.730$–0.816; $T_{wi} = 15$–22°C; $T_{oi} = 50$–75°C; $D_h = 7.6 \times 10^{-3}$–9.6×10^{3} m; $A_f = 3.79 \times 10^{-4}$–$6.98 \times 10^{-4}$ m^2. The constants 729.38 and 1132.2 have the units of kg/m$^{2.19}$ s$^{1.81}$ °C and kg/m$^{2.17}$ s$^{1.83}$ °C, respectively.

REFERENCES

Bird, R., Stewart, W. E. & Lightfoot, E. N. 1960 *Transport Phenomena*. Wiley, New York.
Grover, S. S. & Knudsen, J. G. 1955 *Chem. Engng Prog. Symp. Ser.* **51**, 71–73.

Handlos, A. E. & Baron, T. 1957 Mass and heat transfer from drops in liquid–liquid extraction. *AICHE Jl* **3,** 127–136.

Hinze, J. O. 1955 Fundamentals of the hydrodynamic mechanism of splitting dispersion processes. *AICHE Jl* **1,** 289–295.

Khatib Shahidi, M. 1994 Direct contact heat transfer between two immiscible liquids flowing in a horizontal concentric annulus. M. Sc. thesis, Middle East Technical University, Ankara, Turkey.

Kehat, E. & Sideman, S. 1971 Heat transfer by direct liquid–liquid contact. In *Recent Advances in Liquid–Liquid Extraction*, Chap. 13. Pergamon Press, London.

Köksal, D. 1980 Direct contact heat transfer between immiscible liquids in turbulent pipe flow. M. Sc. thesis, Middle East Technical University, Ankara, Turkey.

Leib, T. M., Fink, M. & Hasson, D. 1977 Heat transfer in vertical annular laminar flow of two immiscible liquids. *Int. J. Multiphase Flow* **3,** 533–549.

Marquardt, D. W. 1963 An algorithm for least squares estimation of nonlinear parameters. *J. Soc. Indust. Appl. Math.* **11,** 431–441.

Moresco, L. L. & Marshall, E. 1980 Liquid–liquid direct contact heat transfer in a spray column. *Trans. ASME.* **102,** 684–687.

Porter, J. W., Goren, S. L. & Wilke, C. R. 1968 Direct contact heat transfer between immiscible liquids in turbulent pipe flow. *AICHE Jl* **14,** 151–158.

Sideman, S. 1966 Direct contact heat transfer between immiscible liquids. In *Advances in Chemical Engineering*, Vol. 6, Chap. 4. Academic Press, New York.

Sideman, S. & Shabatai, H. 1964 Direct contact heat transfer between a single drop and an immiscible liquid medium. *Can. J. Chem. Engng*, **42,** 107–117.

Takahashi, M., Inoue, A., Aoki, S., Aritomi, M. & Endo, H. 1981 Interface heat transfer of horizontal co-current liquid–liquid stratified flow. *Bull. JSME* **24,** 1002–1010.

Yalvaç, S. 1974 Direct contact heat transfer between two immiscible liquids in a pipe. M. Sc. thesis, Middle East Technical University, Ankara, Turkey.

Wilke, C. R., Cheng, C. T., Ledesma, V. T. & Porter, J. W. 1963 Direct contact heat transfer for sea water evaporation. *Chem. Engng Prog.* **59,** 69–75.

APPENDIX

The oil and water mass flow rates were calculated from the following pairs of equations in each pipe set to obtain the desired volume fractions of the phases in each experiment:

Pipe set I: $\dot{m}_o = 0.591581 \times \phi_o \times V_T$,
$\dot{m}_w = 0.69566 \times V_T - 1.180118 \times \dot{m}_o$.

Pipe set II: $\dot{m}_o = 0.393853 \times \phi_o \times V_T$,
$\dot{m}_w = 0.463149 \times V_T - 1.180118 \times \dot{m}_o$.

Pipe set III: $\dot{m}_o = 0.320787 \times \phi_o \times V_T$,
$\dot{m}_w = 0.378567 \times V_T - 1.180118 \times \dot{m}_o$.

The procedure for the derivation of these equations is given for the third pipe set as follows:

$$V_T = (\dot{V}_o + \dot{V}_w)/A_f, \qquad [A1]$$

where

$$\dot{V}_o = \dot{m}_o/\rho_o, \quad \dot{V}_w = \dot{m}_w/\rho_w, \qquad [A2]$$

$$\phi_o = \dot{V}_o/(\dot{V}_o + \dot{V}_w). \qquad [A3]$$

The density of oil at average temperature of 50 °C and the density of water at average temperature of 25 °C are given as:

$$\rho_o = 848 \text{ kg/m}^3,$$

$$\rho_w = 997 \text{ kg/m}^3,$$

$$A_f = 3.79 \times 10^{-4} \text{ m}^2.$$

Using this information and [A1]–[A3], the following equations are obtained for pipe set III:

$$\dot{m}_o = 0.320787 \times \phi_o \times V_T, \quad [A4]$$

$$\dot{m}_w = 0.378567 \times V_T - 1.180118 \times \dot{m}_o, \quad [A5]$$

where the units of mass flow rates $\dot{m}_o$, $\dot{m}_w$, and of V_T are kg/s and m/s, respectively.